

Bunch-by-bunch beam size measurement during injection at Shanghai Synchrotron Radiation Facility

Han-Jiao Chen^{1,2} · Jie Chen¹ · Bo Gao^{1,2} · Yong-Bin Leng^{1,2}

Received: 13 January 2017/Revised: 7 February 2018/Accepted: 8 February 2018/Published online: 25 April 2018
© Shanghai Institute of Applied Physics, Chinese Academy of Sciences, Chinese Nuclear Society, Science Press China and Springer Nature Singapore Pte Ltd. 2018

Abstract Fast beam profile measurement is important in fast beam dynamic behavior investigations. A bunch-by-bunch beam size measurement system, which is presently used to measure horizontal profile, has been developed at the Shanghai Synchrotron Radiation Facility (SSRF) and is capable of measuring bunches within a separation of 2 ns. The system is based on a direct-imaging optical system and high-speed photomultiplier array detector. A high-bandwidth linear signal amplifier and acquisition module have also been designed to process bunch-by-bunch multi-channel signals from the detector. The software resampling technique and principal component analysis method were developed to obtain the synchronized data and enhance the signal-to-noise ratio. The fast injection of transients was successfully captured and analyzed. Moreover, the bunch-by-bunch positions and sizes exhibited strong oscillation after the injection at the horizontal betatron oscillation frequency of the SSRF storage ring, and this demonstrated the bunch-by-bunch measurement capability of our system.

Keywords Beam size measurement · Bunch-by-bunch · Injection process · Principal component analysis

This work was supported by the National Natural Science Foundation of China (No. 11375255).

✉ Yong-Bin Leng
lengyongbin@sinap.ac.cn

¹ Shanghai Institute of Applied Physics, Chinese Academy of Sciences, Shanghai 201800, China

² University of Chinese Academy of Sciences, Beijing 100049, China

1 Introduction

The beam size is a key parameter in the electron storage rings. Additionally, the precision measurement of the beam size plays an important role in the operation and upgrade of the system. The transverse oscillations and transverse emittance enlargement will lead to machine instabilities or even beam loss and can be monitored and alerted by a beam size measurement system. The precise bunch-to-bunch position and size measurement is critical in machine abnormality studies and improvements. In synchrotron radiation (SR) facilities, the beam size in the storage ring affects the beamline brightness, which is of great interest to SR users.

Two trends in beam size measurement are developing: One consists of achieving higher precision, whereas the other consists of achieving higher speed with regard to capturing more details in transient time. In this context, various methods have recently been developed.

The interferometric method of visible SR was originally developed by High Energy Accelerator Research Organization (KEK) [1, 2] and is now been widely applied to small beam size measurements of less than 50 μm in SR accelerators, such as ALBA Synchrotron [3], Stanford Positron Electron Asymmetric Ring (SPEAR3) [4], and Australian Synchrotron (ASLS) [5]. This method is also sufficient for high-energy proton accelerators such as the Large Hadron Collider (LHC) [6]. Moreover, this method can resolve the small beam size to 3–4 μm , with an error of 0.5 μm [7] after system optimization and error control. The wire scanner system is another method of high-resolution beam size measurement in proton and heavy-ion accelerators or Linacs, which is not popular in electron storage rings. The detected beam size is small and has been

measured as approximately 15 μm by the LHC and Super Proton Synchrotron (SPS) [8] and as approximately 5 μm RMS by Stanford Linear Collider (SLC) [9]. By upgrading to a laser wire scanner, the minimum beam size of approximately 4.8 μm was measured with a resolution of 0.3 μm at KEK [10], while the fast wire scanner focused on improving the scan speed in order to measure the transient information as 20 m/s at Advanced Photon Source (APS) with a resolution as low as 10 μm [11].

At the Shanghai Synchrotron Radiation Facility (SSRF) storage ring, the interferometer system and X-ray pinhole system were employed in the beam size measurement. The beam size result from the standard spatial interferometer system was 52.4 μm in the horizontal direction with an error of 5.5%, and a deviation of 2% from the design value of 53.0 μm [12]. A standard X-ray pinhole system was also implemented at the SSRF storage ring, which extracted the 0.8° of dipole radiation. This system consisted of the front end, attenuator, pinhole, yttrium aluminum garnet (YAG) target, camera, and PXI controller. The size after the Gaussian fitting was approximately 70 μm in the horizontal direction and 20 μm in the vertical direction [13].

Normal interferometric, wire scanner, and X-ray pinhole methods have speed limits. Moreover, these methods focus mostly on the precision direction, which is insufficient for the detection of transient transverse information.

In recent years, many studies on turn-by-turn and bunch-by-bunch beam diagnostics have been published. At the Beam Instrumentation (BI) group at SSRF, we have also been focusing on the development of a six-dimensional bunch-by-bunch diagnostic system since 2012. This system consists of the beam position parameters (two dimensions), beam transverse size (two dimensions), beam longitudinal length (one dimension), and beam longitudinal phase (one dimension).

With the bunch-by-bunch diagnostic tool, further transverse and longitudinal instability information can be observed. Additionally, it is an excellent tool for machine impedance and wake-field investigations. Moreover, every bunch is the basic unit of the beam physics research, and the motion information of every bunch will be largely approximate to its natural properties. For light source engineering applications, the diagnostics based on the bunch-by-bunch scale will benefit from the optimization of the injection process and reduce the effects of the insertion devices.

The bunch-by-bunch position was implemented with a resolution of 10 μm and was based on the bunch-by-bunch signal processor and delta over sum algorithm [14, 15]. A two-frequency system was employed for the bunch-by-bunch beam length measurement with large dynamic range of 30 pC–6 nC, and a resolution of less than 0.5 ps calibrated by the Streak Camera [16, 17]. For the bunch

longitudinal phase, we used the rise edge detection method to detect the button BPM signal, which could reach approximately 1 ps [18]. In this paper, the bunch-by-bunch beam size system will be discussed.

Other facilities have also focused on fast beam size measurements in order to achieve turn-by-turn and bunch-by-bunch level. At the Cornell Electron Storage Ring (CESR), a fast beam profile monitor was constructed and installed for turn-by-turn and bunch-by-bunch detection [19]. The system detector was a 32-channel linear array photomultiplier (PMT) manufactured by Hamamatsu Photonics. The horizontal size had a systematic error in comparison with the charge-coupled device (CCD) camera results. With regard to the vertical size, this system can measure 10–100 μm on turn-to-turn and bunch-to-bunch, with 32 InGaAs photodiodes. A turn-by-turn result and 30 bunch-by-bunch bunches with turn average results were presented in their report [20].

A similar system is also underdevelopment at the Kurchatov Institute and the Budker Institute of Nuclear Physics in Russia. They have attempted to use a multi-channel photomultiplier and avalanche photodiode array (APDA) as the detectors. The best published result is a five-bunch averaged for vertical beam profile measurement [21–23].

The Hefei Light Source (HLS) has also attempted to build a fast beam size measurement system, such as that developed by CESR and the Kurchatov Institute. This system considers the feasibility of a logarithmic processing technique applied to the four-channel data from the photomultiplier array detector. The system testing and turn-by-turn data acquisition have also been implemented by using a digitizer and Field-Programmable Gate Array (FPGA) processing [24, 25].

Moreover, the gated camera can be applied to the bunch-by-bunch size measurement and fast transient observation. First, 12 turns of the injected beam have been measured by using a direct-imaging and gated camera in SPEAR3, and an injected-beam damping of 10ms has also been captured with a rotating-mirror sweep across the camera CCD [26]. Similar injection turns were also measured in National Synchrotron Light Source II (NSLS2) [27]. At CESR, they also developed a gated camera system with an interferometer optical conditioning in order to achieve a high-resolution bunch-by-bunch beam size in the single-shot pattern or 30 bunch train [28]. However, the gated camera method cannot receive thousands of turns of information and different bunches in one exposure. Additionally, it needs high-level beam repeatability. With regard to our application, we mostly considered using a high-speed photomultiplier array method in order to achieve fast beam size information.

The major challenges of the actual bunch-by-bunch measurement are the high-speed synchronized multi-

channel signal acquisition and low signal-to-noise from the photomultiplier tubes (PMT) outputs. These were issues that our system needed to address.

In this paper, we discuss the setup of our system, including the front-end optical imaging, high-speed signal acquisition, and data processing, and the experimental results of the beam obtained by injection capture and physical model analysis.

2 Methods and system setup

2.1 System background

The SSRF is a third-generation light source consisting of a 150 MeV linear accelerator, 3.5 GeV booster synchrotron, 3.5 GeV storage ring, and seven phase I beam-lines [29]. Table 1 shows the main beam parameters of the SSRF storage ring.

From the designed parameters of the SSRF storage ring, the time–space requirement of the turn-by-turn measurement was 1.44 μm , and that of the bunch-by-bunch was 2 ns.

A visible radiation diagnostic line has been operated since 2009. It was extracted by a Be mirror in a vacuum tube and reflected by three plane mirrors to our optical experimental room [30]. The radiation in the X-rays passed through the Be mirror and the visible light was reflected on the optical diagnostic room. Thereby, it was applied to the measurement of the horizontal beam size by using the interferometric method and was additionally applied to the bunch length by using a streak camera. However, the Be mirror was distorted mainly in the vertical direction, which contained permanent deformation caused by long-term radiation damage and thermal deformation contributed by the X-ray energy absorption during the machine's operation [31]. The deformation ruined the vertical beam size measurement through the visible light and also affected our bunch-by-bunch size system. Furthermore, the vertical beam size at SSRF was approximately 22 μm , which is smaller than the point-response imaging error of the direct-imaging method based on visible light. Thus, as a first step,

our bunch-by-bunch beam size measurement system focused on the horizontal beam size.

2.2 Optical imaging system

Several optical front-end methods have been suggested and applied to the beam diagnostic region based on the visible light. These include the direct-imaging and interferometric methods. Direct imaging, which is an original and intuitive method to detect the beam shape and size at the source point, was chosen for the bunch-by-bunch measurement because of its low-intensity attenuation and simple system setup. The direct-imaging system contained a concave lens (Lens 1) and convex lens (Lens 2) in order to focus and magnify the light spot and to adopt the pixel size to the photoelectric detector. The optical front-end system diagram is shown in Fig. 1 with the distance between the components.

Two plane mirrors brought the visible light to the optical platform. The light was separated into two paths through a transmissive mirror: One path was toward the interferometer system for horizontal size measurement, and the other one was toward our bunch-by-bunch size measurement. First, a diaphragm was introduced to the optical path as a rectangle of 21.2 mm \times 10.8 mm. It was centered at the middle and low part of the light spot, which was used to correct the deformation of the Be mirror.

The composite lens was adapted from the original vertical interferometer setting. The large focus length (2 m) of the concave lens (Lens 1) imaged the light source located approximately 20 m away within the vicinity of the eye relief lens and was suitable to adjust the convex lens (Lens 2, focus length 24 mm) location in order to find the sufficient object focusing plane of the light source.

An interferometric method was applied to the search for the best composite distance of Lens 1 and Lens 2 in order to focus the light source image. The light point was the unique source in the system. Thus, when the composite lens focused on the light point on the CCD camera, two spots from the double slits were combined together with the highest visibility of the interference fringes. The

Table 1 Main beam parameters of SSRF storage ring

Parameters	Values
Revolution time (μs)	1.44
Beam energy (GeV)	3.5
Harmonic number	720
Bunch space (ns)	~ 2
Longitudinal bunch length @ V_{rf}	14.4 ps @ 4.65 MV
Horizontal beam size at observation point (μm)	53
Vertical beam size at observation point (μm)	22

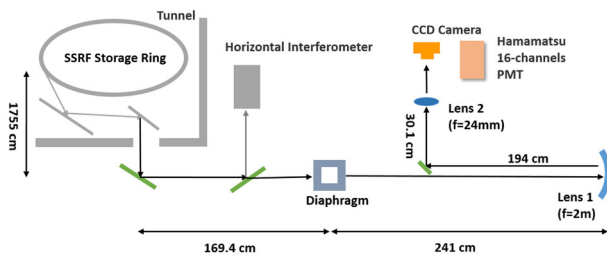


Fig. 1 (Color online) Optical diagram of direct-imaging system

focusing plane of the light point was confirmed by the locations of Lens 1 and Lens 2.

A suitable light spot was obtained by adjusting the distance from Lens 2 linearly after its focal point. Additionally, the amplitude ratio between the object and the image could be calculated based on the schematic of the light path in Fig. 2.

Based on the light path schematic shown in Fig. 2, the size ratio between object S1, and the image at the focal point of Lens 2, S3 was calculated by Eq. (1) as follows:

$$\frac{S1}{S2} = \frac{1965.4 + 200}{220.35}, \frac{S2}{S3} = \frac{3.75}{6.67}, \frac{S1}{S3} \approx 5.5 \quad (1)$$

At the detected position, we obtained a magnified virtual image as S4 or S5 with the distance to the center of Lens 2, whose image size was parallel to the focus point S3. Generally, we placed the PMT array detector approximately 330 cm away from Lens 2. Hence, we had a function to calculate the measured object size $\sigma_{measure}$ with a variable image size σ_x from the CCD results and distance x , as expressed by Eqs. (3) and (2), where σ_{PSF} is the point spread function of the system, M is the amplitude ratio from Eq. (1), D_{S3} is the distance between S3 and the center of Lens 2, and f_2 is the focal length of Lens 2.

$$\sigma_{measure} = \frac{M \cdot (D_{S3} - f_2) \sigma_x}{x - f_2} \quad (2)$$

$$\sigma_{real} = \sqrt{\sigma_{measure}^2 - \sigma_{PSF}^2} \quad (3)$$

For the optical system spread function (PSF) calibration, we used an experimental method based on the size result of the interferometer system. From the CCD result, the image size at the focus point S3 was approximately 14.6 μm and was equal to the object beam size of 80.3 μm . The size

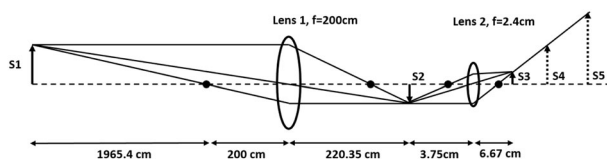


Fig. 2 Schematic of light path

result from the interferometer system was 53 μm , and the system PSF contribution was approximately 60.3 μm .

2.3 Signal conditioning and acquisition

For the bunch-by-bunch measurement, the response speed of the photoelectric detector is one of the key parameters and was less than 2 ns for the no pulse tailing influence on the next bunch signal. The photomultiplier array was manufactured by Hamamatsu Photonics. In our application, H10515B with 16 channels in one dimension was selected. The specifications of the detector are listed in Table 2.

The signals of the 16 channels were extracted from the two-row pins in the center of the back panel, and the negative high-voltage supply for the photomultiplier array was provided to two separated pins below by the Hamamatsu C4900 power supply module, which provided a variable value from -200 to -1200 V depending on the surrounding resistance connection.

A front-end pickup board was designed for interface conversion from the plug pins to the SMA connectors with impedance matching and isometric routing. Four high-bandwidth and high-gain amplifiers were adopted for front-end signal magnification in order to match the data acquisition system input requirements. These amplifiers were also manufactured by Hamamatsu Photonics with a bandwidth of 50 k–1.5 GHz and gain of 36 dB, so as to ensure a coaxial design. As the first step of system configuration and measurement exploration, only the four-channel signals of the photomultiplier array were picked up for the investigation of size measurement and instability. Hence, we used an Agilent DSO9064A oscilloscope for the four-channel data acquisition with an analog bandwidth of

Table 2 Specifications of Hamamatsu H10515B photomultiplier array detector [32]

Parameters	Values
Effective area per channel (mm)	0.8×16
Channel pitch (mm)	1
Spectral range (nm)	300–800
Peak wavelength (nm)	420
Gain	1×10^6
Rise time (ns)	0.6
Fall time (ns)	1.691
Transit time spread (FWHM) (ns)	0.18
Pulse linearity per channel ($\pm 2\%$) (mA)	0.8
Cross talk (%)	3
Supply voltage (Vdc)	-800

600 MHz and maximum sampling rate of 5 GHz. The layout of the signal front-end processing and acquisition is shown in Fig. 3 with the front and back panel of the PMT array detector.

2.4 Data processing

Because of the oscilloscope's limited data storage, we could store approximately 2 μm to the 20 ms waveform of four channels at a maximum sampling rate of 5 GS/s, which is equal to approximately 1380–13,880 turns in the normal operation mode at SSRF. The basic data processing workflow based on the oscilloscope data was divided into three parts: data resampling, data optimization, and parameter calculation.

The data processing was carried out with the MATLAB software, and the workflow is shown in Fig. 4.

Data resampling is a software-synchronized sampling process for achieving the minimum point of every bunch, based on an actual RF frequency. The real data period was calculated from the Fast Fourier Transform (FFT) result, and the valley value of every signal pulse was picked up by using the spline interpolation method based on real period.

Data optimization includes data reshaping in order to carry out the separation in bunches and turns and to achieve noise reduction. The signal-to-noise ratio (SNR) was strongly improved by the principal component analysis (PCA) method in our application [33]. This will be demonstrated by actual beam examples in the following section.

The final process was Gaussian fitting, based on four data points from the signal intensities of the four PMT array channels. The bunch position and bunch size were derived from parameters μ and σ of the Gaussian fitting result.

3 Injection transient study

An injection phenomenon was captured by the four-channel setup of the bunch-by-bunch size measurement system during the SSRF normal operation mode, whose beam current was approximately 260 mA, whereas the charge of every bunch was approximately 0.78 nC. During

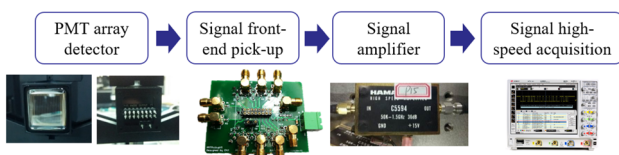


Fig. 3 (Color online) Layout of signal detection (PMT array), front-end processing (signal pickup and amplifiers), and acquisition (oscilloscope)

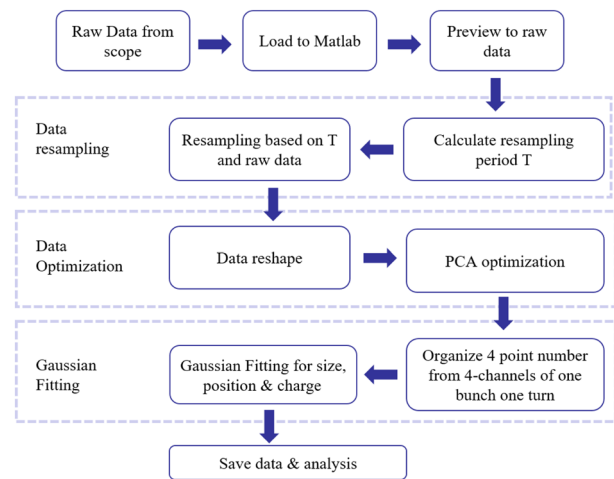


Fig. 4 Data software processing workflow

the injection, the transverse feedback system was OFF. The filling pattern consisted of four long beam chains, and each chain contained approximately 120 filled and 60 blank buckets. The filling pattern is shown in Fig. 5.

When the injection event occurred, the output signal of the PMT array channels would be slightly larger than the normal average value. The method of capturing the injection status consisted of setting a larger trigger level than the normal value (approximately 20 mV) and the single operation mode in the oscilloscope. The injection event would be locked after being generated with this setting.

3.1 Data acquisition and processing

The raw signal from the oscilloscope is shown in Fig. 6 with a detailed and overview waveform. The figure shows a strong amplitude oscillation, which was interplaced between the left and right channels. The chosen channels of the PMT array were channels 7, 8, 10, and 11, the distance between channels 7 and 8 and channels 10 and 11 was 1 mm, while that of channels 8 and 10 was 2 mm, with consideration to the appropriate four points chosen on the Gaussian curve. The center of the light spot was placed

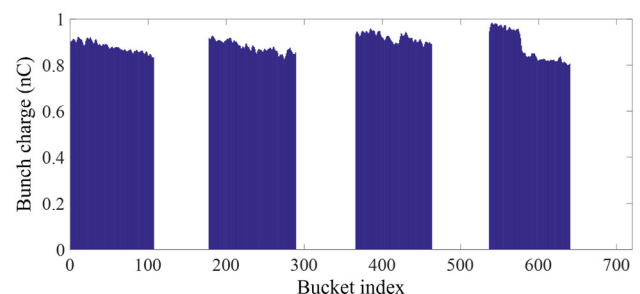


Fig. 5 (Color online) Normal filling pattern of SSRF operation (four bunch chains, approximately 66.7% duty radio)

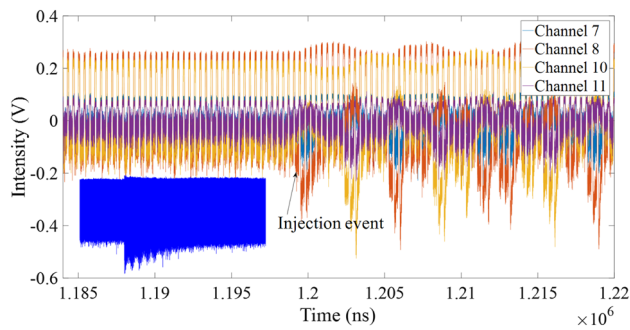


Fig. 6 (Color online) Raw signal data from oscilloscope with detailed plot and overview

around channel 9. Hence, channels 8 and 10 exhibited high intensity, whereas channels 7 and 11 exhibited low intensity near the edge of the light spot.

The minimum point of every bunch in the four channels was resampled by our synchronous resampling algorithm. Subsequently, the PCA algorithm was introduced to the data processing workflow and contributed to the outstanding noise reduction performance and injection oscillation expression. The comparison of the resampled data before and after the PCA algorithm is shown in Fig. 7. The injection oscillation of a single bunch in turns appears to be very pronounced in Fig. 7b.

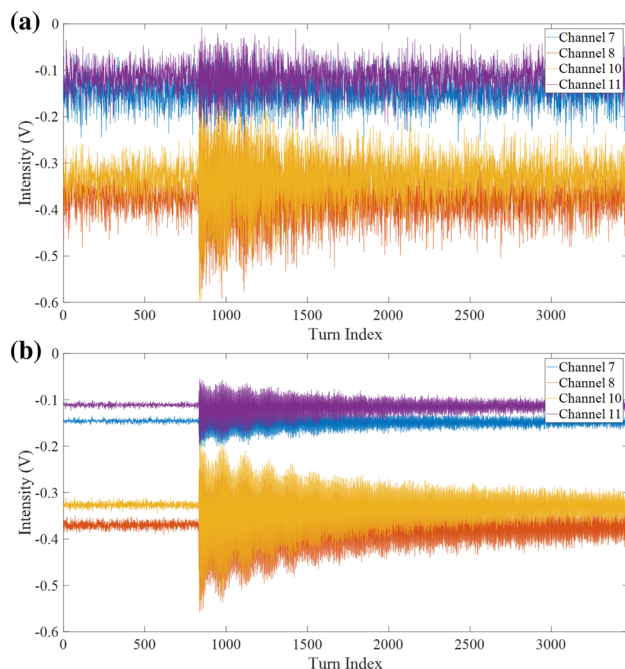


Fig. 7 (Color online) Statistic noise removed by PCA method: **a** before PCA, **b** after PCA

3.2 Results and discussion

After data processing, described in Sect. 2, the bunch size and position results of every bunch in turns were calculated as a matrix in combination with the bunch index in rows and the turn index in columns. We picked up the initial oscillation amplitude of the position in every bucket, and the result is shown in Fig. 8.

The betatron oscillation of the bunches was introduced by two sources: the mismatch of the injection kicker field and the wake-field effects of the previous bunches. Hence, all the buckets exhibited different position oscillation amplitude as different contributions from these two parts, as shown in Fig. 8. The largest oscillation occurred at bunch #1, whereas the smallest oscillation occurred at bunch #231. Hence, we analyzed the turn-by-turn oscillation behaviors of the bunch position and bunch size of these two bunches in the time domain as typical results of all of the filling buckets in the storage ring. The obtained results are shown in Fig. 9.

The behavior of the kicker field mismatching contribution was a typical damping oscillation with the highest amplitude at the injection and attenuation to the normal value, as shown in the position oscillation of bunch #1 in Fig. 9a, and was mostly contributed by this function.

While the wake-field effects enlarged the oscillation amplitude after the injection as a wake-field transmission, the instability item of bunch #231 was mostly contributed by the wake-field effects, and its waveform started to enlarge at approximately 500 turns after the injection. The oscillation amplitude tended toward a stable value after turn #1500, since it was affected by the SSRF storage ring damping. The position oscillation pattern of the kicker field mismatching and wake-field effects from the PMT array signals were also confirmed by the results of the BPM buttons. This has also been discussed in detail in previously published papers [33, 34].

The size results of bunch #1 and bunch #231 were also the combined effects of the kicker field mismatching and wake field and were in good agreement with the position

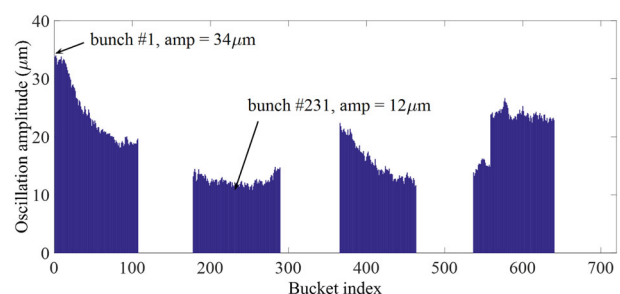


Fig. 8 (Color online) Initial position oscillation amplitude of every bucket

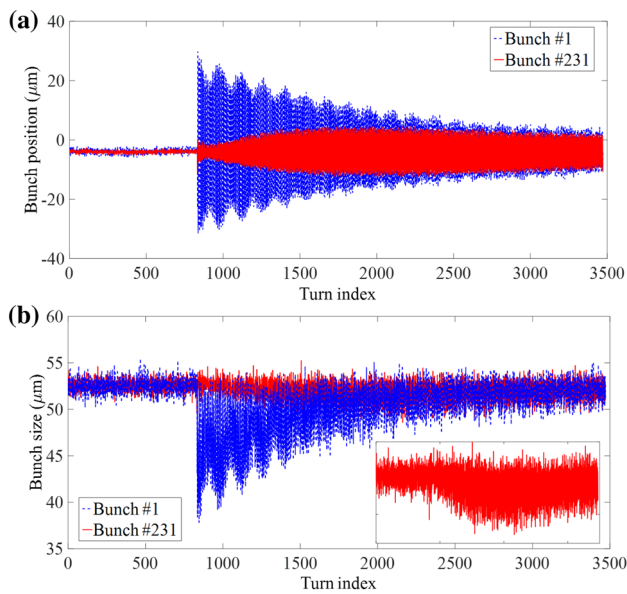


Fig. 9 (Color online) Turn-by-turn oscillation of position and size of bunch #1 and bunch #231 in time domain: **a** bunch position result, **b** bunch size result

results. The wake-field effects in bunch #231 were not as obvious because of the low resolution of the size measurement, which has been magnified in Fig. 9b. Later, however, it also exhibited the envelope of the wake-field effects and stable amplitude.

The points made in the above discussion can be fortified by the spectra analysis of the position and size results. Additionally, we could determine the different behaviors of the position and size in the spectra shown in Fig. 10.

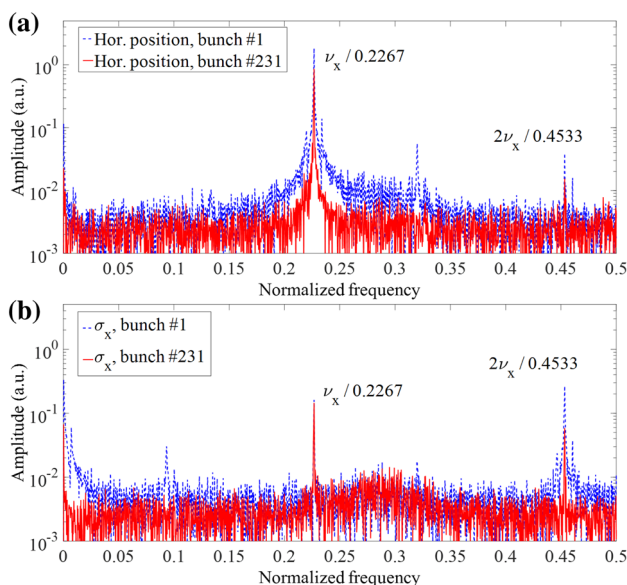


Fig. 10 (Color online) Spectra of bunch position and size result: **a** bunch position, **b** bunch size

The position spectra of bunch #1 and bunch #231 were all contained in the horizontal tune frequency and its second harmonic frequency. The main contribution was the tune frequency, with the two synchrotron sidebands appearing around it as the main kicker field mismatching contribution to bunch #1. Moreover, there were no obvious sidebands at the same position of the bunch #231 result, where mainly wake-field effects were observed.

The same tune frequency and second harmonic frequency were also detected on the size spectra. However, the peak amplitude occurred at the second harmonic frequency of the bunch #1 result with the two synchrotron sidebands, as the kicker field mismatching effects in the size that were contained in the direction vector. Moreover, there was a formant near the DC frequency in bunch #1. With regard to the bunch #231 results, the wake-field contribution did not focus strongly on the second harmonic frequency and exhibited similar amplitude between the tune and the second harmonic frequency with no synchrotron sidebands.

If we combined the size spectra of all the buckets in one figure, a plot known as the waterfall plot would be as shown in Fig. 11. The refilled buckets were from #574 to #579 and exhibited larger amplitude than the surrounding buckets.

The distribution of the bunch transverse profile in the storage ring can be equivalent to a Gaussian distribution. The integral area of the Gaussian distribution will not change as a stable bunch charge. Hence, the product of σ and the center intensity of the Gaussian distribution is a constant. If the σ of the Gaussian distribution increases, the center intensity will decrease, and vice versa when σ decreases. This would be an appropriate method to verify the reliability of our system. Here, σ means the bunch size and the center intensity is the amplitude of the spot center in the PMT array. Figure 12 shows the correlation between the size and center intensity of the #1 image of the bunch in turns. The large bunch center intensity had a small bunch size and low center intensity with a large bunch size that matched the theoretical analysis result and supports the

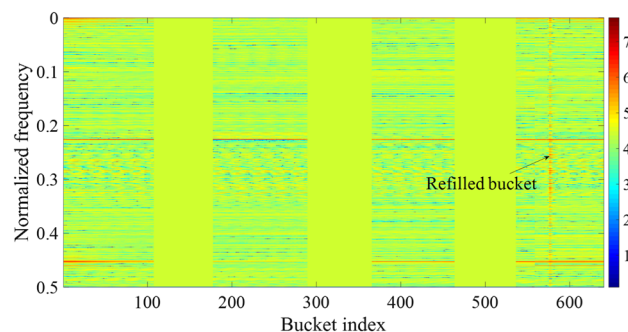


Fig. 11 (Color online) Size spectra waterfall plot of all buckets

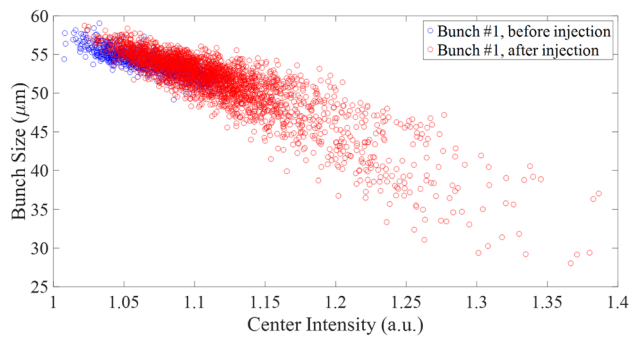


Fig. 12 (Color online) Correlation results between bunch size and center intensity

reliability of the bunch-by-bunch beam size measurement system.

4 Conclusion

A four-channel bunch-by-bunch beam size measurement system was designed, built, and implemented at SSRF. The injection transient was successfully captured with a high-sampling-rate oscilloscope. The bunch size oscillated between 38 and 53 μm , and the bunch position oscillation was measured from -30 to 28 μm . The betatron oscillation characteristics were introduced by the kicker field mismatching, and the wake-field effects were analyzed from the position and size results. Additionally, the position result was confirmed by the bunch-by-bunch transverse position system results with the button pickup [33]. The spectra and correlation results demonstrated that the system was capable of turn-by-turn and bunch-by-bunch measurement. Moreover, the fast beam size measurements are excellent tools for injection and other fast transient investigations.

The resolution of the four-channel signal fitting is a limitation of the current system configuration and originated mostly from the multi-channel high bandwidth and sampling rate data acquisition limitation. A further system upgrade will complete the 12–16 channel readout based on synchronized 3–4 digitizers with enough bandwidth and sampling-rate as a data acquisition solution. It will also be a part of a six-dimensional bunch-by-bunch diagnostic system at SSRF and will serve as a beam size measurement solution.

Acknowledgements The authors thank Dr. De-Chong Zhu from Institute of High Energy Physics (IHEP) for his suggestion with regard to overcoming the effect of the Be mirror distortion. We also thank the operation team of SSRF for its assistance in conducting the beam experiment.

References

1. T. Mitsuhashi, T. Naito, In: Proceedings of 6th European Particle Accelerator Conference, 22. (Stockholm, Sweden, 1998), pp. 165–1657
2. T. Naito, T. Mitsuhashi, Very small beam-size measurement by a reflective synchrotron radiation interferometer. *Phys. Rev. ST Accel. Beams* **9**, 122802 (2006). <https://doi.org/10.1103/PhysRevSTAB.9.122802>
3. L. Torino, U. Iriso, In: Proceedings of 3rd International Beam Instrumentation Conference. (Monterey, CA, USA, 2014), pp. 374–379
4. J. Corbett, W. Cheng, A.S. Fisher et al., In: Proceedings of 23rd Particle Accelerator Conference. (Vancouver, BC, Canada, 2009), pp. 4018–4020
5. M.J. Boland, T. Mitsuhashi, T. Naito, et al., In: Proceedings of 1st International Beam Instrumentation Conference. (Tsukuba, Japan, 2012), pp. 566–570
6. G. Trad, E. Bravin, A. Goldblatt, et al., In: Proceedings of 5th International Beam Instrumentation Conference. (Barcelona, Spain, 2016), pp. 583–588
7. T. Mitsuhashi, In: Proceedings of 6th International Particle Accelerator Conference. (Richmond, VA, USA, 2015), pp. 3662–3667
8. J. Emery, B. Dehning, C.M. Pereira, et al., In: Proceedings of 2014 IEEE Conference on Control Applications. (Antibes, France, 2014), pp. 1139–1145
9. R. Fulton, J. Haggerty, R. Jared et al., A high resolution wire scanner for micron-size profile measurements at the SLC. *Nucl. Instrum. Methods A* **274**, 37–44 (1989). [https://doi.org/10.1016/0168-9002\(89\)90362-8](https://doi.org/10.1016/0168-9002(89)90362-8)
10. T.B. Stewart, A.B. Grahame, B. Gary et al., Micron-scale laser-wire scanner for the KEK Accelerator Test Facility extraction line. *Phys. Rev. ST Accel. Beams* **13**, 122801 (2010). <https://doi.org/10.1103/PhysRevSTAB.13.122801>
11. T. Moore, N.I. Agladze, I.V. Bazarov et al., Fast wire scanner for intense electron beams. *Phys. Rev. ST Accel. Beams* **17**, 022801 (2014). <https://doi.org/10.1103/PhysRevSTAB.17.022801>
12. J. Chen, K. Ye, Y. Leng, Development of Shanghai Synchrotron Radiation Facility synchrotron radiation interferometer. *High Power Laser Part. Beams* **23**, 179–184 (2011)
13. Y.B. Leng, G.Q. Huang, M.Z. Zhang et al., The beam-based calibration of an X-ray pinhole camera at SSRF. *Chin. Phys. C* **36**, 80–83 (2012)
14. Y. Yang, Y.B. Leng, Y.B. Yan et al., Development of the bunch-by-bunch beam position acquisition system based on BEEcube. *Nucl. Sci. Tech.* **27**, 47 (2016). <https://doi.org/10.1007/s41365-016-0035-4>
15. Y.B. Leng, Y. Yang, N. Zhang, In: Proceedings of 2nd International Beam Instrumentation Conference. (Oxford, UK, 2013), pp. 746–748
16. L.W. Duan, Y.B. Leng, R.X. Yuan et al., Injection transient study using a two-frequency bunch length measurement system at the SSRF. *Nucl. Sci. Tech.* **28**, 93 (2017). <https://doi.org/10.1007/s41365-017-0247-2>
17. H.J. Chen, L.W. Duan, Y.B. Leng, et al., In: Proceedings of 6th International Beam Instrumentation Conference. (Grand Rapids, MI, USA, 2017)
18. Y.M. Zhou, Y.B. Leng, H.J. Chen et al., In: Proceedings of 8th International Particle Accelerator Conference. (Copenhagen, Denmark, 2017), pp. 341–344
19. S.T. Wang, D.L. Rubin, C.R. Strohmman, et al., In: Proceedings of 4th International Particle Accelerator Conference. (Shanghai, China, 2013), pp. 849–851

20. J.P. Alexander, A. Chatterjee, C. Conolly et al., Vertical beam size measurement in the CESR-TA e+ e- storage ring using x-rays from synchrotron radiation. *Nucl. Instrum. Methods A* **748**, 96–125 (2014). <https://doi.org/10.1016/j.nima.2014.02.040>
21. A.V. Bogomyagkov, V.F. Gurko, A.N. Zhuravlev et al., New fast beam profile monitor for electron–positron colliders. *Rev. Sci. Instrum.* **78**, 043305 (2007). <https://doi.org/10.1063/1.2720729>
22. A.I. Kotelnikov, A.D. Khilchenko, V.L. Dorohov et al., In: Proceedings of 5th International Particle Accelerator Conference. (Dresden, Germany, 2014), pp. 3617–3619
23. V. Dorokhov, A. Khilchenko, A. Kotelnikov et al., In: Proceedings of 5th International Beam Instrumentation Conference. (Barcelona, Spain, 2016)
24. C.C. Cheng, Y.Y. Xiao, B.G. Sun et al., In: Proceedings of 4th International Particle Accelerator Conference. (Shanghai, China, 2013), pp. 556–558
25. C.C. Cheng, Ph.D. Thesis, University of Science and Technology of China, (2016)
26. W. Cheng, J. Corbett, A. Fisher et al., In: Proceedings of 23rd Particle Accelerator Conference. (Vancouver, Canada, 2009), pp. 4015–4019
27. W. Cheng, B. Bacha, H. Xu et al., In: Proceedings of 3rd International Beam Instrumentation Conference. (Monterey, CA, USA, 2014), pp. 369–373
28. S.T. Wang, R. Holtzapfel, D.L. Rubina, Single-shot beam size measurements using visible-light interferometry at CESR. *Nucl. Instrum. Methods A* **847**, 34–41 (2017). <https://doi.org/10.1016/j.nima.2016.11.014>
29. SSRF, <http://e-ssrf.sinap.cas.cn/>
30. J. Chen, K.R. Ye, Y.B. Leng, In: Proceedings of 1st International Beam Instrumentation Conference. (Tsukuba, Japan, 2012), pp.1–5
31. B. Gao, Y.B. Leng, H.J. Chen et al., In: Proceedings of 8th International Particle Accelerator Conference. (Copenhagen, Denmark, 2017), pp. 332–334
32. Hamamatsu Photonics. <http://www.hamamatsu.com/jp/en/product/alpha/P/3002/H10515B-20/index.html> H10515B-20 specifications
33. Z. Chen, Y. Yang, Y.B. Leng et al., Wakefield measurement using principal component analysis on bunch-by-bunch information during transient state of injection in a storage ring. *Phys. Rev. ST Accel. Beams* **17**, 112803 (2014). <https://doi.org/10.1103/PhysRevSTAB.17.112803>
34. Y. Yang, Y.B. Leng, Y.B. Yan et al., Injection performance evaluation for SSRF storage ring. *Chin. Phys. C* **39**, 110–114 (2015)